

# An Advanced Modulation Scheme Emphasizing Neutral Point Ripple Suppression using Predictive Control for Three-Level NPC Converters in Aircraft Electric Starter Generator Applications

Chen Li\*, Tao Yang\*, Giovanni Lo Calzo†, Serhiy Bozhko\*, Chris Gerada\*, Patrick Wheeler\*

\*Power Electronics, Machines, Control(PEMC) group, University of Nottingham, NG7 2RD, Nottingham, UK

†Dyson Ltd, SN16 0RP, Malmesbury, UK

<Chen.Li@nottingham.ac.uk, Tao.Yang@nottingham.ac.uk>

**Keywords:** Electric Starter Generator, Surface Mount PMSM, Three Level Neutral Point Clamped Inverter, Neutral Point Ripple Suppression.

## Abstract

Electrical starter/generator (ESG) system is one of the key innovations of more-electric aircraft initiative. The ESG cranks the engine and accelerates it up to self-sustained speed using electric energy (starter mode) and then runs as a generator to supply onboard loads. Three-level neutral point clamped (NPC) converter have been identified as a preferable choice for ESG applications due to high power quality as well as efficiency. However, the application of three-level NPC converter in the ESG systems has certain challenges. One of which is the low frequency neutral point voltage ripple, especially in generation mode when running at high speeds such that the flux weakening control is required. The paper proposes an advanced modulation scheme which can balance the neutral point voltage for the full range of speeds and loading conditions. Using the proposed technique, zero neutral point voltage deviation within each switching period is achieved by introducing a sharing factor computed in a deadbeat predictive approach. The proposed technique is validated with simulation results.

## 1 Introduction

Being a key technology for the More Electric Aircraft (MEA) notion, the aircraft electric starter generator (ESG) technology has attracted increasing amount of research interest. Among reported topologies, the Permanent Magnet Synchronous Machine (PMSM) based topology is the one showing most potential in terms of its size, weight, power density, efficiency and simplicity [1][2].

The proposed ESG system operates as an interface between the aircraft engine shafts and the aircraft DC power system. As shown in Figure. 1, the rotor of the PMSM is connected to the engine shaft. During the engine start, the DC/AC converter inverts DC power and drives the PMSM to accelerate the engine shaft (compressor) up to ignition speed. In generation mode, the engine shaft can be seen as a large inertia, where

mechanical power is extracted and rectified to electric power to supply various onboard loads.

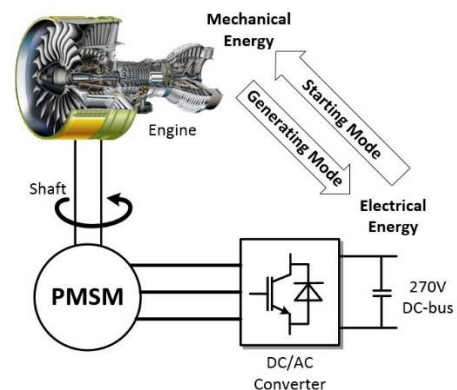


Fig. 1. PMSM based aircraft electric starter generator system

For the DC/AC converter, three-level Neutral Point Clamped (3L-NPC) is chosen over the classic two-level inverter for its advantages in efficiency and operation under high fundamental frequency [3].

However for 3L-NPC converter, the DC-link neutral point voltage imbalance has always been a problem. As imbalance of the DC-link capacitor voltages may endanger the capacitor by overvoltage and cause significant output voltage distortion on the AC side. Many methods have been reported in the past, one category being common-mode voltage injection [3][4][6] combined with carrier based pulse width modulation (CPWM). This group of methods inject common-mode voltage by modifying the modulating waveform, so that the average neutral point current is biased towards one direction, achieving neutral point balancing. Alternatively, for 3L-NPC converter with space vector modulation (SVM), the redundancy of the small vectors is exploited to maintain the neutral point balancing. As opposite small vectors differ in common-mode voltage, these two methods share some similarity, however both methods become less effective under reduced power factor condition. There are also harmonic injection methods reported, such as six harmonic voltage injection [7] and even-order current harmonics injection [8]. Both methods showing desirable performance under low power factor condition.

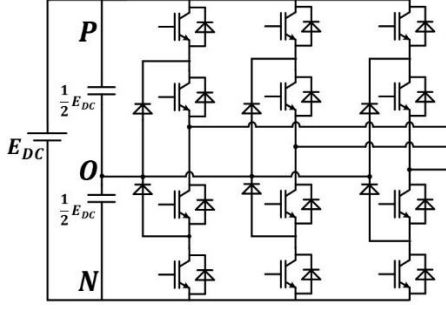


Fig. 2. Three-Level Neutral Point Clamped Converter

Apart from neutral point voltage balancing, one further issue of the 3L-NPC converter is the 3<sup>rd</sup> harmonic voltage ripple of the neutral point voltage under high modulation index [9]. As the neutral point voltage ripple causes distortion on the output side, it should be suppressed to a lower level by installing a pair of larger capacitors, assuming no additional hardware is implemented. However, having large DC-link capacitors would significantly increase the size and weight of the converter, which is not desirable for transport related applications such as MEA.

To reduce the 3<sup>rd</sup> harmonic voltage ripple, a modified space vector modulation technique namely the virtual space vector modulation is proposed. During high modulation index operation, such method ties the duty cycles of two small vectors and the medium vector together, formulating the virtual space vector [10] (VSV). As the virtual space vector connects the DC-link neutral point to all three phases for the same amount of time, the average neutral point current for the virtual vector is zero, thus significantly reducing the 3<sup>rd</sup> harmonic ripple. However, such method increases the switching loss as well as AC side THD. Many hybrid modulation techniques are also proposed to achieve a trade-off between the advantages of the conventional SVM method and the virtual SVM method [11][12][13]. As the aim of such hybrid solution is to suppress the 3<sup>rd</sup> harmonic voltage ripple in the neutral point, the average neutral point current is used to determine whether to use the conventional SVM method or to use VSV based SVM method. The transition process between the two methods have also been improved to achieve a seamless transition with minimum influence to the stability of the control.

As the aircraft starter generator system operates in a wide range of conditions, the performance of the modulation method would have to be optimized for the full operation range. Under light load operation, the power flowing between the machine and the converter is small and therefore a low power factor is expected. High rotation speed of the engine shaft implies the PMSM is constantly operating in flux weakening operation with a high fundamental frequency, therefore the modulation index for the power converter is constantly near unity. Furthermore, a low pulse ratio is also expected as the switching frequency of the converter is limited. Very few existent SVM techniques can deliver desirable performance under such operating condition.

This paper features a modified SVM technique aided by predictive control, aiming at suppression of the neutral point

voltage ripple with full power factor and modulation index range, thus minimizing the size of DC-link capacitors.

## 2 System Model & Control

### 2.1 PMSM Model

For the starter-generator machine, a Surface Mount Permanent Magnet Synchronous Machine is used, the voltage equations in synchronous reference frame are presented as follows:

$$V_{abc} = R_s \cdot I_{abc} + \frac{d\lambda_{abc}}{dt} \quad (1)$$

Where

$$R_s = \begin{bmatrix} r_s & 0 & 0 \\ 0 & r_s & 0 \\ 0 & 0 & r_s \end{bmatrix} \quad (2)$$

And flux linkage is expressed by:

$$\lambda_{abc} = L_s \cdot I_{abc} + \lambda_{PM}^s \quad (3)$$

Where

$$L_s = \begin{bmatrix} L_{ls} + L_{ms} & -\frac{1}{2}L_{ms} & -\frac{1}{2}L_{ms} \\ -\frac{1}{2}L_{ms} & L_{ls} + L_{ms} & -\frac{1}{2}L_{ms} \\ -\frac{1}{2}L_{ms} & -\frac{1}{2}L_{ms} & L_{ls} + L_{ms} \end{bmatrix} \quad (4)$$

And

$$\lambda_{PM}^s = \lambda_{PM} \begin{bmatrix} \sin \theta_r \\ \sin(\theta_r - \frac{2}{3}\pi) \\ \sin(\theta_r + \frac{2}{3}\pi) \end{bmatrix} \quad (5)$$

Where  $L_{ls}$  represents the leakage inductance of stator windings,  $L_{ms}$  represents the mutual inductance of stator windings,  $\lambda_{PM}$  represents the permanent magnet flux and  $\theta_r$  represents the rotor flux position of the PMSM.

The voltage and flux equations can be transformed from  $abc$  frame into stationary reference frame using Clarke transformation. The voltage equations in  $\alpha\beta$  reference frame is:

$$\begin{bmatrix} v_\alpha^s \\ v_\beta^s \end{bmatrix} = R_s \begin{bmatrix} i_\alpha^s \\ i_\beta^s \end{bmatrix} + \frac{d}{dt} \begin{bmatrix} \lambda_\alpha^s \\ \lambda_\beta^s \end{bmatrix} \quad (6)$$

And flux linkage being:

$$\begin{bmatrix} \lambda_\alpha^s \\ \lambda_\beta^s \end{bmatrix} = L_s \begin{bmatrix} i_\alpha^s \\ i_\beta^s \end{bmatrix} + \lambda_{PM}^r \begin{bmatrix} \cos \theta_r \\ \sin \theta_r \end{bmatrix} \quad (7)$$

Park transformation transforms quantities from  $\alpha\beta$  reference frame to synchronous reference frame:

$$\begin{bmatrix} v_d^r \\ v_q^r \end{bmatrix} = R_s \begin{bmatrix} i_d^r \\ i_q^r \end{bmatrix} + L_s \frac{d}{dt} \begin{bmatrix} i_d^r \\ i_q^r \end{bmatrix} + \frac{d}{dt} \begin{bmatrix} \lambda_d^r \\ \lambda_q^r \end{bmatrix} \quad (8)$$

And

$$\begin{bmatrix} \lambda_d^r \\ \lambda_q^r \end{bmatrix} = L_s \omega_r \begin{bmatrix} -i_q^r \\ i_d^r \end{bmatrix} + \lambda_{PM}^r \omega_r \begin{bmatrix} 0 \\ 1 \end{bmatrix} \quad (9)$$

## 2.1 ESG Control

The control structure of the ESG system is very close to a vector controlled PMSM drive, where three phase currents are transformed into synchronous reference frame and controlled separately using classic PI controllers with decoupling applied.

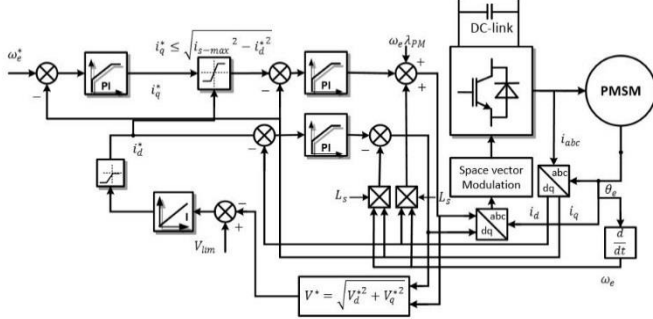


Fig. 3. ESG control structure in starting mode

In starting mode operation, the ESG system applies a high starting torque to the engine shaft and accelerates it to ignition speed. Initially the d-axis current reference is set to zero and the q-axis current reference is set by speed controller. After the PMSM exceeds base speed, the d-axis current reference is generated by integrating the difference between the output voltage reference and converter voltage limit. This implies the modulation index of the converter would be near unity after this point of the operation. In flux weakening operation, if overall current approach the converter current limit (set by thermal limitations), the de-fluxing d-axis current would be given priority whereas the q-axis current reference would be sacrificed.

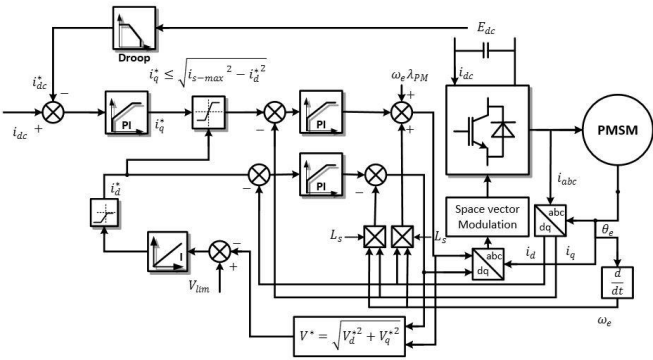


Fig. 4. ESG control structure in generation mode

In generation mode, the power flows from the engine shaft to the onboard DC power system of the plane. Synchronous reference frame current regulators as well as the flux weakening controller are retained. However the q-axis current reference is set by a droop controller to achieve load sharing between multiple parallel ESG systems on a single DC bus [14], [15]. It should be noted that in this context the current flowing from the converter to the machine is in the positive direction, therefore the q-axis current of the PMSM in generating condition is always negative.

## 3 Low Frequency Ripple

## 3.1 Principle of SVM Operation

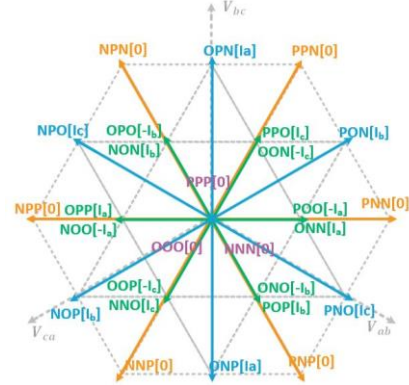


Fig. 4. Space vector diagram for three level converters

Three level converters offer a total number of 27 possible voltage space vectors. Shown in Fig. 4, voltage vectors with magnitudes of  $\frac{2}{3}V_{DC}$  are large vectors, voltage vectors which reside at the centre are null vectors, these vectors do not connect any phases to the neutral point. Alternatively, small vectors come in pairs with opposite neutral point current directions.

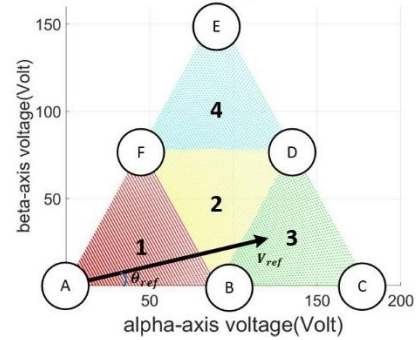


Fig. 5. Nearest Three Vector (NTV-SVM) illustration

Conventional space vector modulation technique divides the space vector hexagon in Fig. 4 into six sectors, each sector contains four regions. Take the third region of the first sector within the space vector hexagon as an example, the conventional NTV-SVM method generates the reference vector inside this region by three adjacent available space vectors, hence B, C and E. Duty cycles of correspondent vectors can be calculated with voltage-time-area based on:

$$V_{ref} = d_B V_B + d_C V_C + d_D V_D \quad (10)$$

$$d_B + d_C + d_D = 1 \quad (11)$$

## 3.2 Source of Ripple

Using the conventional space vector modulation as an example, the charge flows into and out of the DC-link neutral point under high modulation index can be illustrated by mapping the variation of phase currents and medium vector duty cycles. The charge is represented by current-time-area (ITA, actually current time duty cycle).

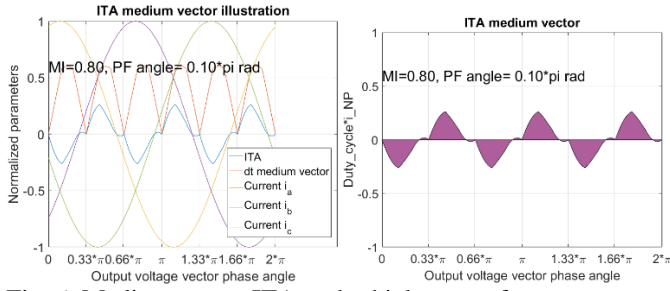


Fig. 6. Medium vector ITA under high power factor

Given a modulation index of 0.8 and a power factor of 0.1pi, the variation of medium vector neutral point current-time-area in a fundamental cycle is illustrated in Fig. 6. Results show that the way neutral point is connected within a fundamental cycle naturally forms a variation of charge at three times the fundamental frequency. At relatively high power factor conditions, the charge variation induced by medium vector can be compensated by small vectors.

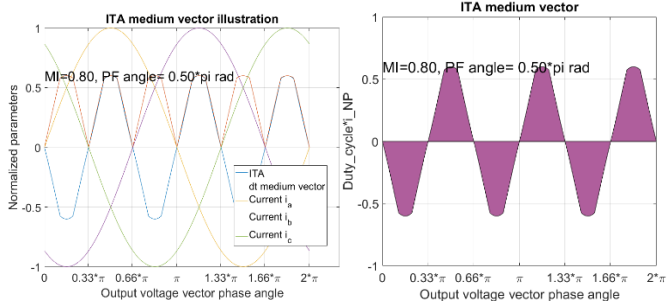


Fig. 7. Medium vector ITA under low power factor

At a lower power factor condition shown in Fig. 7, where the power factor is 0.5pi, the charge variation under such condition reveals a clear variation three times of the fundamental frequency, which explains the source of the low frequency neutral point voltage ripple under lower power factor conditions.

## 4 Modulation Scheme

### 4.1 Original Modulation Method

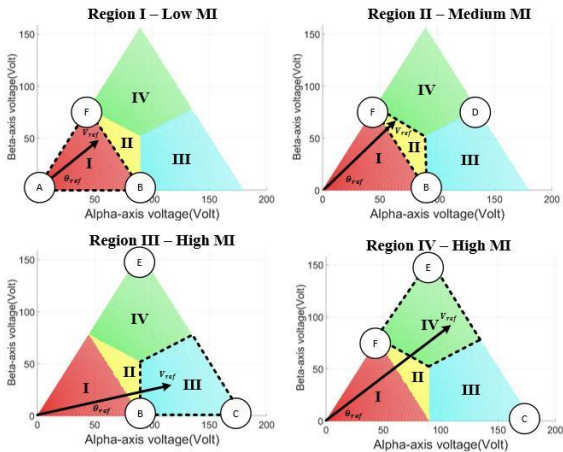


Fig. 8. Previously develop method

To suppress the third harmonic voltage ripple and possible DC-link voltage imbalance, one modulation approach recently developed and published is briefly introduced here.

The modulation method given in Fig. 8 selects three voltage space vectors in a switching period just like the NTV-SVM method. However, to avoid excessive 3<sup>rd</sup> harmonic voltage ripple in the neutral point, the use of the medium vector is forbidden at modulation index region, which are region III and region IV. The polarity of the small vector is determined based on the measured neutral point voltage and neutral point current calculated from phase currents or the q-axis current. For the first case, the selection table is Table I, where  $+i_{NP}$  and  $-i_{NP}$  represents the small vector with its neutral point current kept the same or inverted.

Table I, small vector selection table

$\Delta V_{DC}$	$i_{NP}$	$i_{NP} < 0$	$i_{NP} > 0$
$\Delta V_{DC} > 0$		$+i_{NP}$	$-i_{NP}$
$\Delta V_{DC} < 0$		$-i_{NP}$	$+i_{NP}$

### 4.2 Neutral point voltage ripple

With this method, at high modulation index, the possible low frequency voltage ripple can indeed be suppressed. Nevertheless, it should be noted that in both region III and IV, hence the high modulation index region, the selected voltage space vectors are always two large vectors and one adjacent small vector, among which only the adjacent small vector affects the neutral point voltage. Therefore, could be a case where instantaneous neutral point voltage imbalance is increased due to the use of the method.

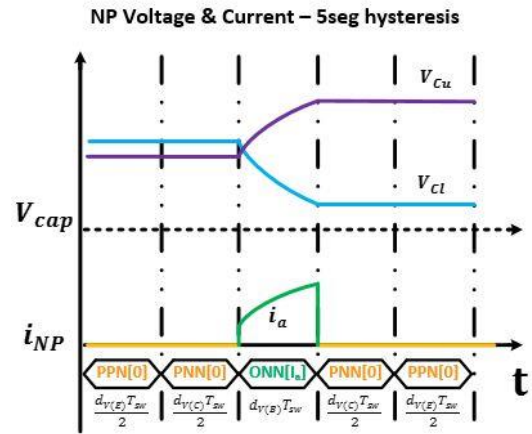


Fig. 9. Possible downside of the previously proposed method

As illustrated in Fig. 9, assuming the reference voltage vector generated by control resides in region III of the first sector as in Fig. 5 and the bottom left condition in Fig. 8, phase-a is connected to the neutral point, therefore the neutral point current equals to phase a current. The condition of neutral point voltage imbalance and polarity of neutral point current dictates the small vector ONN should be chosen to drive the neutral point voltage to a balanced state. However, as the magnitude of voltage imbalance is small, the control action applied would actually result in a relatively large overshoot and create an even larger neutral point voltage imbalance.

Given the neutral point voltage is controlled in a hysteresis fashion by the small vector in high modulation index operating condition, such effect would be rampant.

### 4.3 Predictive approach for sharing factor calculation

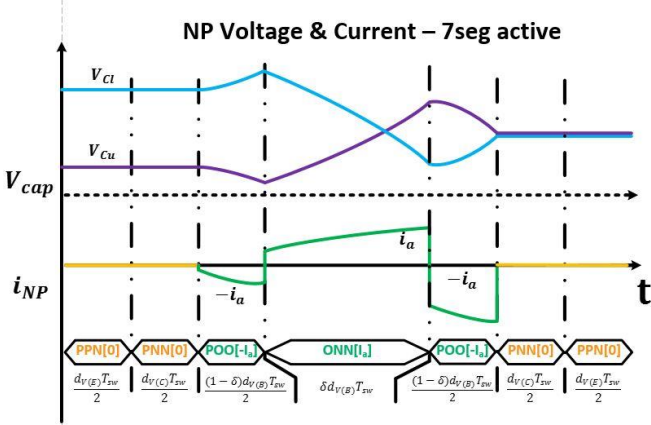


Fig. 10. Modified space vector modulation method

To address the neutral point voltage overshoot issue caused by the hysteresis, a simple solution is to apply the small vector with both polarities. Given in Fig. 10, the same condition given in Fig. 9 is applied, the same voltage space vectors with the same duty-cycles are selected. For the small vector, both patterns of vector B in sector I (bottom left of Fig.8) are applied. The duty cycle of the small vector is divided by a sharing factor  $\delta$ , which leads to zero neutral point voltage imbalance at the end of the switching period.

The performance of such method is dependent on the accuracy of the sharing factor  $\delta$ . The charge difference between the upper and the lower DC-link capacitors  $\Delta Q_{NP}$  under a certain voltage imbalance can be computed as:

$$\Delta Q_{NP} = (V_{cap\_H} - V_{cap\_L})C_{cap} \quad (12)$$

Where  $V_{cap\_H}$  and  $V_{cap\_L}$  represents measured voltages of the upper and the lower DC-link capacitors respectively and  $C_{cap}$  represents their capacitance. For the small vector, with given duty-cycle  $d_s$  and average phase current  $i_{NP}$ , the variation of neutral point charge can also be calculated as:

$$\Delta Q_S = d_s T_S i_{NP} \quad (13)$$

The term  $T_S$  is the time of a single switching period. With existing charge variation  $\Delta Q_{NP}$  and the future variation of charge  $\Delta Q_S$  calculated, the sharing can then be obtained by:

$$\delta = \frac{1}{2} \left( 1 + \frac{\Delta Q_{NP}}{\Delta Q_S} \right) \quad (14)$$

In most of previous reported methods, the quantities required to compute the control actions are assumed to be constant. However this assumption would not be accurate under low pulse ratio condition. To compensate the inaccuracies caused by having a low pulse ratio as well as sampling delay. A 1.5

step prediction method shown in Figure. 11 can be adopted to improve the accuracy of the sharing factor. At the time instant  $t(k)$ , quantities including phase currents, neutral point voltages are sampled, and control action  $V_{out}(k-1)$  generated in the previous interrupt service routine (ISR) is applied. As the control action  $V_{out}(k-1)$  is known, the quantities at time instant  $t(k+1)$  hence the next ISR can be predicted. With the control actions  $V_{out}(k)$  generated by executing control algorithm, the average neutral point current for the small vector selected during  $t(k+1)$  can be obtained by predicting machine phase currents by  $0.5T_S$ , hence at time instant  $t(k+1.5)$ . As the voltage space vectors applied is half-wave symmetrical, predicting the quantities at  $t(k+1.5)$  from the predicted quantities at  $t(k+1)$  can be done by using only half of the output voltage  $V_{out}(k)$ .

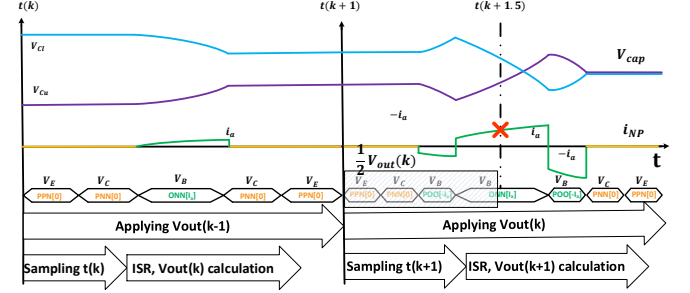


Figure. 11. Proposed SVM with 1.5 step prediction

In the synchronous reference frame, with the voltage and flux equations given in (8) and (9), the derivatives of d-axis and q-axis currents can be obtained by:

$$\begin{bmatrix} \frac{di_d^r}{dt} \\ \frac{di_q^r}{dt} \end{bmatrix} = \frac{1}{L_s} \left( \begin{bmatrix} v_d^r \\ v_q^r \end{bmatrix} - R_s \begin{bmatrix} i_d^r \\ i_q^r \end{bmatrix} + L_s \omega_r \begin{bmatrix} i_q^r \\ -i_d^r \end{bmatrix} - \lambda_{PM} \omega_r \begin{bmatrix} 0 \\ 1 \end{bmatrix} \right) \quad (15)$$

Currents at the next time instant are:

$$\begin{bmatrix} i_{d_{k+1}}^r \\ i_{q_{k+1}}^r \end{bmatrix} = T_S \begin{bmatrix} \frac{di_d^r}{dt} \\ \frac{di_q^r}{dt} \end{bmatrix} + \begin{bmatrix} i_{d_k}^r \\ i_{q_k}^r \end{bmatrix} \quad (16)$$

The rotor flux position variation during sampling period can be compensated by:

$$\theta_{r_{k+1}} = T_S \omega_r + \theta_{r_k} \quad (17)$$

The neutral point current can then be mapped by current switching function from predicted phase currents obtained by inverse dq-transformation:

$$i_{NP_{k+1}} = [M_a \quad M_b \quad M_c] \begin{bmatrix} \cos \theta_{r_{k+1}} & -\sin \theta_{r_{k+1}} \\ \cos(\theta_{r_{k+1}} - \frac{2}{3}\pi) & -\sin(\theta_{r_{k+1}} - \frac{2}{3}\pi) \\ \cos(\theta_{r_{k+1}} + \frac{2}{3}\pi) & -\sin(\theta_{r_{k+1}} + \frac{2}{3}\pi) \end{bmatrix} \begin{bmatrix} i_{d_{k+1}}^r \\ i_{q_{k+1}}^r \end{bmatrix} \quad (18)$$

## 5 Simulation

Simulation results for the proposed 4th harmonic current injection method is obtained with an ESG model implemented in PLECS/Simulink environment. The 3L-NPC converter is supplied by a 270V dc-link, a pair of 600uF capacitors

selected, the switching frequency is 16kHz. The PMSM driven by the 3L-NPC has pole number of 6, phase resistance of  $1.1 \times 10^{-3}$  Ohm, phase inductance of 99e-6 Henry and PM flux of 0.0364 Vs/rad. At 20krpm of speed, the ESG is in generating mode with no load, the modulation index is high as deep flux-weakening is required. Results given in Fig. 12 demonstrates the accuracy of the 1.5step prediction.

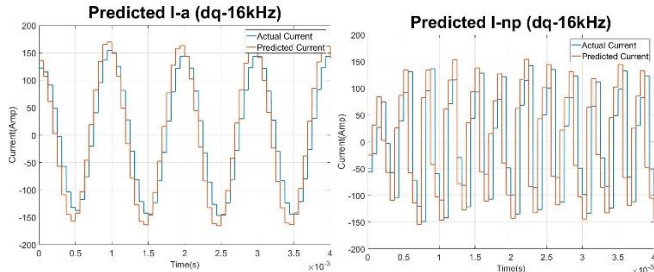


Figure 12. Predicted phase current & neutral point current

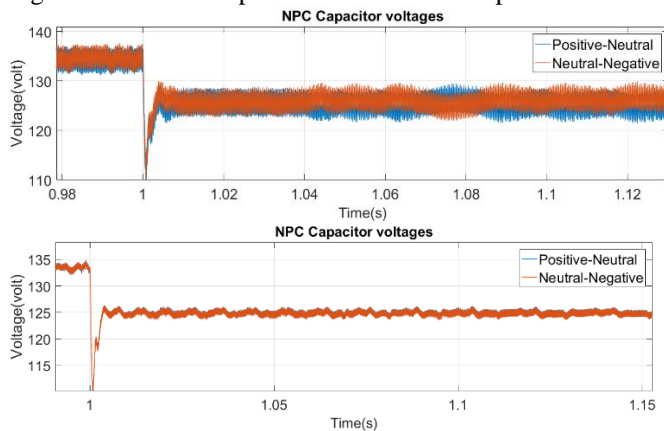


Figure 13. Neutral point voltage ripple

From no-load generating operation, a 15kw of load is connected to the DC-link and created a droop of DC-link voltage. The variation of DC-link capacitor voltages under the transient is presented in Figure 13, where the top trace is collected when conventional modulation approach is used, and the bottom one shows the performance of the proposed method, where the voltage ripple is reduced.

## 6 Conclusion

This paper has introduced a modified space vector modulation technique for three-level neutral point clamped converters with aircraft electric starter generator system. The usage of the medium vector is restricted at high modulation index region, leaving only large vectors and small vectors available. To minimize the neutral point voltage ripple, both patterns of the selected small vector are applied with their duty-cycles divided by a sharing factor. A 1.5 step predictive approach is adopted to ensure the accuracy of the sharing factor. The performance of the proposed method is validated by simulation results collected in a PLECS/Simulink model.

## Acknowledgements

This paper has introduces a modified space vector modulation technique for three-level neutral point clamped

converters The study has been supported by Clean Sky 2 (Systems ITD, project EMINEO), European H2020 program.

## References

- [1] S. Bozhko, S. S. Yeoh, F. Gao, and C. Hill, "Aircraft starter-generator system based on permanent-magnet machine fed by active front-end rectifier," in *IECON 2014 - 40th Annual Conference of the IEEE Industrial Electronics Society*, 2014, pp. 2958–2964.
- [2] P. Wheeler and S. Bozhko, "The More Electric Aircraft: Technology and challenges.," *IEEE Electr. Mag.*, vol. 2, no. 4, pp. 6–12, Dec. 2014.
- [3] M. Schweizer, T. Friedli, and J. Kolar, "Comparative Evaluation of Advanced 3-phase 3-level Inverter/Converter Topologies against 2-level Systems," *IEEE Trans. Ind. Electron.*, vol. 60, no. 12, pp. 5515–5527, 2013.
- [4] Y. Zhang, J. Li, X. Li, Y. Cao, M. Sumner, and C. Xia, "A Method for the Suppression of Fluctuations in the Neutral-Point Potential of a Three-Level NPC Inverter With a Capacitor-Voltage Loop," *IEEE Trans. Power Electron.*, vol. 32, no. 1, pp. 825–836, Jan. 2017.
- [5] C. Newton and M. Sumner, "Neutral point control for multi-level inverters: theory, design and operational limitations," in *IAS '97. Conference Record of the 1997 IEEE Industry Applications Conference Thirty-Second IAS Annual Meeting*, vol. 2, pp. 1336–1343.
- [6] C. Wang and Y. Li, "Analysis and calculation of zero-sequence voltage considering neutral-point potential balancing in three-level NPC converters," *IEEE Trans. Ind. Electron.*, vol. 57, no. 7, pp. 2262–2271, 2010.
- [7] H. Akagi and T. Hatada, "Voltage Balancing Control for a Three-Level Diode-Clamped Converter in a Medium-Voltage Transformerless Hybrid Active Filter," *IEEE Trans. Power Electron.*, vol. 24, no. 3, pp. 571–579, Mar. 2009.
- [8] M. Marchesoni, P. Segarich, and E. Soressi, "A new control strategy for neutral-point-clamped active rectifiers," *IEEE Trans. Ind. Electron.*, vol. 52, no. 2, pp. 462–470, 2005.
- [9] N. Celanovic and D. Boroyevich, "A comprehensive study of neutral-point voltage balancing problem in three-level neutral-point-clamped voltage source PWM inverters," *IEEE Trans. Power Electron.*, vol. 15, no. 2, pp. 242–249, Mar. 2000.
- [10] S. Busquets-Monge, J. Bordonau, D. Boroyevich, and S. Somavilla, "The nearest three virtual space vector PWM - a modulation for the comprehensive neutral-point balancing in the three-level NPC inverter," *IEEE Power Electron. Lett.*, vol. 2, no. 1, pp. 11–15, Mar. 2004.
- [11] C. Xia, H. Shao, Y. Zhang, and X. He, "Adjustable proportional hybrid SVPWM strategy for neutral-point-clamped three-level inverters," *IEEE Trans. Ind. Electron.*, vol. 60, no. 10, pp. 4234–4242, 2013.
- [12] G. I. Orfanoudakis, M. A. Yuratich, and S. M. Sharkh, "Nearest-vector modulation strategies with minimum amplitude of low-frequency neutral-point voltage oscillations for the neutral-point-clamped converter," *IEEE Trans. Power Electron.*, vol. 28, no. 10, pp. 4485–4499, 2013.
- [13] A. Choudhury, P. Pillay, and S. S. Williamson, "DC-Bus Voltage Balancing Algorithm for Three-Level Neutral-Point-Clamped (NPC) Traction Inverter Drive With Modified Virtual Space Vector," *IEEE Trans. Ind. Appl.*, vol. 52, no. 5, pp. 3958–3967, Sep. 2016.
- [14] F. Gao, S. Bozhko, A. Costabeber, C. Patel, P. Wheeler, C. I. Hill, and G. Asher, "Comparative Stability Analysis of Droop Control Approaches in Voltage-Source-Converter-Based DC Microgrids," *IEEE Trans. Power Electron.*, vol. 32, no. 3, pp. 2395–2415, Mar. 2017.
- [15] F. Gao, S. Bozhko, A. Costabeber, G. M. Asher, and P. W. Wheeler, "Control Design and Voltage Stability Analysis of a Droop-Controlled Electrical Power System for More Electric Aircraft," *IEEE Trans. Ind. Electron.*, pp. 1–1, 2017.